Biomechanically-Constrained 4D Estimation of Myocardial Motion

Hari Sundar, Christos Davatzikos, and George Biros

Section for Biomedical Image Analysis, Department of Radiology,
University of Pennsylvania

Abstract. We propose a method for the analysis of Magnetic Resonance (MR) cardiac images with the goal of reconstructing the motion of the ventricular walls. The main feature of our method is that the inversion parameter field is the active contraction of the myocardial fibers. This is accomplished with biophysically-constrained, four-dimensional (space plus time) formulation that aims to complement information that can be gathered from the images by a priori knowledge of cardiac mechanics and electrophysiology. *Our main hypothesis is that by incorporating biophysical information, we can generate more informative priors and thus, more accurate predictions of the ventricular wall motion.* In this paper, we outline the formulation, discuss the computational methodology for solving the inverse motion estimation, and present preliminary results using synthetic data. We integrate an in-house spatially non-uniform octree meshing scheme with an adjoint-based inversion solver. The overall method uses patient-specific MR data and fiber information to reconstruct the motion. In these preliminary tests, we verify the implementation and conduct a parametric study to test the sensitivity of the model to material properties perturbations, model errors, and incomplete and noisy observations.

Imaging can help in the diagnosis of cardiac masses, cardiomyopathy, myocardial infarcion, and valvular disease. Cine Magnetic Resonance Imaging (cine-MRI) is emerging as the method of choice for diagnosing a variety of cardiovascular disorders [1,2]. Alternative specialized pulse sequences (e.g., tagged cine-MRI) can create rich image features, but they have lower resolution and signal-to-noise ratio. In addition, computational challenges limit analysis to 3D (2D $\times$ time) motion estimation, where in fact 4D analysis would be preferable [3,4].[1] Segmentation of the ventricles and the myocardium is the first step toward quantitative functional analysis of cine-MRI data. However, segmentation is time consuming, thereby limiting clinical throughput [5]. Moreover, sometimes accuracy is limited by long-axis motion, and inter and intra-observer variability [6].

Related work. To address these problems in motion reconstruction, one of the main thrusts in recent research has been 4D motion estimation using

[1] Other modalities, like stimulated-echo, and phase-contrast MR can be used but are problematic with respect noise-to-signal ratio, resolution, and acquisition time.

biomechanical models.[2] There is significant work on the integration of imaging with cardiovascular mechanics. In [7], a piecewise linear composite biomechanical model was used to determine active forces and the strains in the heart based on tagged MRI information. In [8] and [9], echocardiography and MR images were combined with biomechanical models for cardiac motion estimation. Interactive segmentation was combined with a Bayesian estimation framework that was regularized by an anisotropic, passive, linearly elastic, myocardium model. The authors recognized the importance of neglecting active contraction of the left ventricle. In [10,11,12], the need for realistic simulations and the need for inversion and data assimilation was outlined. In [13], Kalman filters were used to recover the initial state of the heart and spatial abnormalities. That method however, is difficult to generalize to nonlinear inversion with time-dependent inversion parameters.

Contributions In this article, we propose a biomechanically-constrained motion estimation algorithm that has the potential to partially address motion estimation problems. It is based on a PDE-constrained optimization formulation that explicitly couples raw image information with a biomechanical model of heart. We discuss the formulation, numerical implementation, and we present preliminary verification tests that confirm the potential of the method. *The novelty of our approach is on the formulation and the algorithmics (solvers and parallel implementation).* The main features of our scheme are (1) a patient-specific image-based inversion formulation for the active forces; (2) a multigrid-accelerated, octree-based, adaptive finite-element forward solver that incorporates anatomically-accurate fiber information; and (3) an adjoint/Hessian-based inversion algorithm. This work builds on our previous work on massively parallel octree-based methods [14], and large-scale inverse algorithms for acoustic and elastic scattering [15]. Our method requires (1) segmentation of the blood pool and myocardium at the initial frame to assign material properties and (2) a deformable registration to a template to map fiber-orientations the template to the patient. This is done using our in-house tensor mapping method [16].

1 Formulation of the inverse problem

The basic premise of our formulation is the following: The heart motion is induced by the active forces in the myocardium. If we knew the exact biomechanical model for the myocardial tissue (constitutive law, geometry, fiber orientations, material properties for the heart and surrounding tissues, endocardial tractions due to blood flow) and the active stretching time-space profile, then we could solve the so-called "*forward problem*" for the displacements of the myocardial tissue. Similarly, if we knew the displacements at certain locations in the myocardium, we could solve the so-called "*inverse problem*" to reconstruct active forces so that the motion due to the reconstructed forces matches the observed one. More generally, we have cine-MRI data but not the displacements. We can

[2] Due to space limitations we do not attempt to review all related literature.

still invert for the displacements—by solving a biomechanically-constrained image registration problem.

In this context, an abstract formulation of the myocardium motion estimation problem is given by

$$\min_{u,s} \mathcal{J}(I_t, I_0, u) \quad \text{subject to} \quad \mathcal{C}(u, s) = 0. \tag{1}$$

Here, $I_t := I_t(x,t)$ is the cine-MR image sequence with x, t denoting the space-time coordinates, $I_0 := I(x,0)$ is the initial frame (typically end-diastole), $u := u(x,t)$ is the *displacement* (motion), $s = s(x,t)$ is the active fiber contraction, and $\mathcal{C}$ is the forward problem operator. Also, $\mathcal{J}$ is an image similarity measure functional. This is a classical PDE-constrained inverse problem [15]. Notice that there is no need for elastic, fluid, or any kind of regularization for u. It is constrained through the biomechanical model $\mathcal{C}$.[3]

Objective function (Operator $\mathcal{J}$). For the purposes of this paper, we assume a preprocessing step, in which we apply a keypoint-matching algorithm [17] on the data I_t: we compute point-correspondences for all time frames, i.e., $d_j(t) := u(x_j, t)_{i=1}^{M}$ at M points.[4] Then, the objective function is given by

$$\mathcal{J} := \int_0^1 (Qu - d)^2 \, dt := \int_0^1 \sum_{i=1}^{M} (u(x_j, t) - d_j(t))^2 \, dt, \tag{2}$$

where Q is the so called spatial observation operator.

Forward problem (Operator $\mathcal{C}$). We make several approximations. we assume a linear isotropic inhomogeneous viscoelastic material for the myocardium; we ignore the geometric nonlinearities in both material response and active forces; we model the blood pool as an incompressible material with very small stiffness and strong damping. We recognize that these are very strong assumptions but the model is meant to be driven by image data and assist in the motion reconstruction. More complex models can be incorporated—if clinical validation suggests the need to do so. In addition to the constitutive assumptions, we assume a model for the active forces: given the fiber contractility s as a function of space and time, we define the active stretch tensor $U = 1 + s\, n \otimes n$, whose divergence results in a distributed active force of the form $\text{div}(s\, n \otimes n)$. Taken together, these assumptions result in the following form for $\mathcal{C}$:

$$M\ddot{u}(t) + C\dot{u}(t) + Ku(t) + As(t) = 0 \quad t \in (0,1). \tag{3}$$

Using a Ritz-Galerkin formulation, with ϕ and ψ basis functions for u and s respectively, the expressions for M, K and $A(n)$ are given by $M_{ij} = \int \mathrm{I}(\phi_i \phi_j)$, $K = \int (\lambda + \mu) \nabla\phi_i \otimes \nabla\phi_j + \mu \mathrm{I}(\nabla\phi_i \cdot \nabla\phi_j)$, $A_{ij} = \int (n \otimes n) \nabla\phi_i \psi_j$, and $C =$

[3] However, one can show that the problem is ill-posed on s. Here we regularize by discretization of s.

[4] We are implementing an image registration functional that does not require such point-correspondences.

$\alpha M + \beta K$, with α and β viscous-damping parameters. Here, $\otimes$ is the outer vector product, λ and μ are the Lamé constants, and I is the 3D identity matrix. Equation (3) is derived by the Navier linear elastodynamics equation [18]. The domain of spatial integration (for M, K, and A) is the unit cube, corresponding to the cine-MR domain. In our formulation, we solve for the motion of *all the tissue* in the MR images. At the outer boundaries of the cube we impose homogeneous Neumann boundary conditions. Also, we assume zero displacements and velocities as initial conditions.

Inverse problem. The inverse problem is stated by (1) where $\mathcal{J}$ is given by (2) and $\mathcal{C}$ is given by (3). By introducing Lagrange multipliers p, the first-order optimality conditions for (1) can be written as:

$$\begin{aligned} M\ddot{u}(t) + C\dot{u}(t) + Ku(t) + As(t) = 0, \quad \dot{u}(0) = u(0) = 0, \\ M\ddot{p}(t) - C\dot{p}(t) + Kp(t) + Q^T(Qu - d) = 0, \quad \dot{p}(1) = p(1) = 0, \\ A^T p(t) = 0. \end{aligned} \tag{4}$$

The second equation is the so-called "*adjoint problem*". Equation (4) consists of a system of partial-differential equations for u (cardiac motion), p (adjoints), and s (active fiber contraction). It is a 4D boundary value problem since we have conditions prescribed at both $t = 0$ and $t = 1$.

Discretization and solution algorithms. We discretize the forward and adjoint problems in space using a Ritz-Galerkin formulation. We have developed a parallel data-structure and meshing scheme, discussed in [14]. The basis functions are trilinear, piecewise continuous polynomials. In time, we discretize using a Newmark scheme. The overall method is second-order accurate in space and time. The implicit steps in the Newmark scheme are performed using Conjugate Gradients combined with a domain-decomposition preconditioner in which the local preconditioners are incomplete factorizations. The solver and the preconditioner are part of the PETSc package [19].

For these particular choices of objective function and forward problem the inverse problem (4) is linear in p, u, and s. We use a reduced space approach in which we employ a matrix-free Conjugate-Gradients algorithm for the Schur-complement of s—also called the (reduced) Hessian operator. Each matrix-vector multiplication with the Hessian requires one forward and one adjoint cardiac cycle simulation. Furthermore, one can show that the Hessian is ill-conditioned. Thus, the overall computational cost of the inversion is high. We are developing efficient multigrid schemes for the inverse problem. Details of this approach can be found in [15]. To reduce the computational cost for the calculations in the present paper, we used a reduced-order model for s in which ψ is a product of B-splines in time and radial functions in space (Gaussians). This discretization not only does it allow acceleration of the inverse problem but it introduces a model error since the synthetic "ground truth" is generated using a full resolution fiber model and the inversion is done using the reduced resolution fiber model. This allows to perform preliminary tests on the sensitivity of our method to model errors.

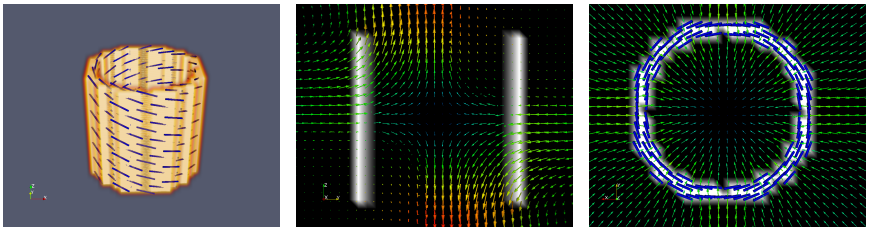

(a) (b) (c)

Fig. 1: *(a) The cylindrical model with the fiber orientations, (b) the deformations developed within the myocardium as a result of the contraction, and (c) the deformations displayed along with the fiber orientations (blue line segments).*

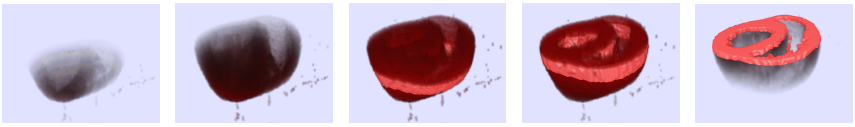

(a) (b) (c) (d) (e)

Fig. 2: *The activation function used in the synthetic model of the heart. The activation function starts at the apex and moves to the base of the ventricles.*

2 Results

We first describe the set of experiments performed to validate the numerical accuracy of the forward cardiac model. We used a simple cylindrical model where the fiber orientations are circumferential and downwards, leading to the generation of radial forces and deformations. This model is shown in Figure 1 The second model used was constructed from a MR image of a human heart. The fiber orientation was obtained from ex-vivo Diffusion Tensor (DTI) images of the heart. In order to drive the forward model, we generated forces by propagating a synthetic activation wave from the apex to the base of the ventricles. Snapshots of this activation wave at different phases of the cardiac cycle are shown in Figure 2. The fiber orientation, the myocardial forces and the resulting deformations within the myocardium are shown at different slices and time points in Figures 3 and 4. For both models we selected a Poisson's ratio $\nu = 0.45$ and a Young's modulus of 10 kPa for the myocardial tissue and 1 kPa for the surrounding tissue and ventricular cavity. Raleigh damping ($C = \alpha M + \beta K$) was used with parameters $\alpha = 0$ and $beta = 7.5 \times 10^{-4}$.

We use the cylinder model to study the convergence of the forward solver by comparing the results obtained from the numerical solver with the analytical solution. The solution was obtained for discretizations corresponding to regular grids 32^3, 64^3 and 128^3 and 50, 100, and 200 time steps respectively. The

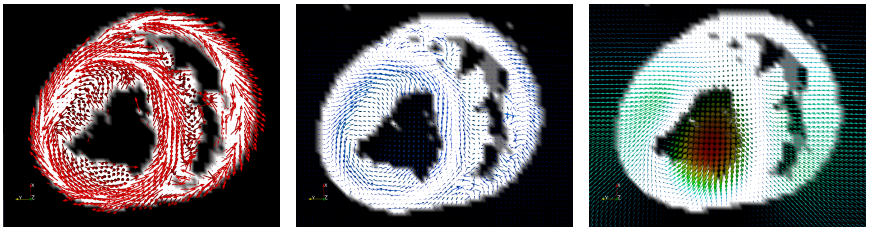

(a) (b) (c)

Fig. 3: *(a) The orientation of the cardiac fibers, (b) the forces developed within the myocardium as a result of the contraction of the fibers, and (c) the resulting deformations within the myocardium.*

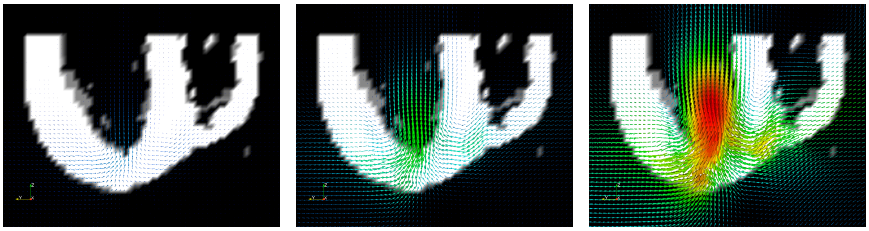

(a) (b) (c)

Fig. 4: *The deformations induced by the propagation of the activation from the apex to the base.*

use of octrees for meshing reduced the number of elements significantly. We observed $\mathcal{O}(h^2)$ convergence, where h is the grid size. These results, along with the number of processors used and the time for the computation are tabulated in Table 1. For the inverse problem, we validate the error in the estimation of

Grid Size	Number of Octants	Number of Processors	Relative Error $\|\cdot\|_2$	Time (secs)
32^3	7719	1	7.63×10^{-2}	81
64^3	52K	8	1.91×10^{-2}	101
128^3	256K	64	4.77×10^{-3}	113

Table 1: *Convergence results for the forward model using the cylinder geometry. All errors are with respect to the analytical solution.*

the activations for different degrees of parametrization using the radial basis. In all cases, the number of b-Spline basis per spatial location were fixed to 5 degrees of freedom. The relative error in the estimation of the activation for a 64^3 grid is for spatial parametrizations of 2^3, 4^3 and 8^3 is tabulated in Table 2. Ground truth activations are generated using a 2. These runs were done on 64 processors. In addition, we investigated the error in the estimation when only

Basis Size	Relative Error $\|\cdot\|_2$	Time
2^3	1.31×10^{-1}	36 mins
4^3	5.67×10^{-2}	$\approx$ 5 hrs
4^3	1.12×10^{-1}	108 mins
8^3	9.66×10^{-2}	141 mins

Table 2: *Error in recovery of activation for increasing number of radial basis functions. By changing the inversion solver accuracy, we can accelerate the calculation without compromising accuracy (e.g., the 4^3 calculation).*

Observations	Relative Error $\|\cdot\|_2$
Full	5.36×10^{-2}
1/8	6.21×10^{-2}
1/64	8.51×10^{-2}

Table 3: *Error in the recovery of activation with partial observations of the displacements. Errors are reported on the cylinder model for a grid size of 32 with 4^3 basis functions.*

partial observations are available. We compared estimations based on full and sparse observations with 12% and 6% samples against the analytical solutions. These results are tabulated in Table 3. In order to assess the sensitivity of the motion estimation framework, we estimated the motion for the synthetic model of the heart at a grid size of 64 with a radial basis parametrization of 4^3 by adding noise to the system. We added a 5% random error on the estimates of the fiber orientation and to the material properties of the myocardium. In addition, we added a 1% noise to the true displacements. The system converged and the relative error (L_2) increased from 5.67×10^{-2} to 9.43×10^{-2}.

3 Conclusions

We presented a method for cardiac motion reconstruction. We integrate cine-MR images and a biomechanical model that accounts for inhomogeneous tissue properties, fiber information, and active forces. We presented an inversion algorithm. We will able to solve problems that involve 300 million unknowns (forward and adjoint in space-time) in a couple of hours on 64 processors—a modest computing resource. The potential of the method as multicore platforms become mainstream is significant.

The limitations of our current implementation (but not the method) is the assumptions of linear geometric and material response and the potential bias due to template-based fibers that does not account for anatomical variability, that is still requires some preprocessing of the initial frame to assign material properties and fiber orientation, that assumes zero residual stresses and initial conditions, and that it does not include an electrophysiology model.

Our on-going work includes transition to an intensity-based image-registration inversion (in which case we need to solve a nonlinear inversion), further verification of the method by comparing to manually-processed real data, and its clinical validation by reconstructing motions of normal and abnormal populations and conducting statistical analysis. Among the many open problems are the level of required model complexity for clinically relevant motion reconstructions, the bias of the fibers, the sensitivity to the values of the material properties, and the sensitivity to the image similarity functional.

References

1. Castillo, E., Lima, J.A.C., Bluemke, D.A.: Regional myocardial function: Advances in MR imaging and analysis. Radiographics **23** (2003) S127–S140
2. Shah, D.J., Judd, R.M., Kim, R.J.: Technology insight: MRI of the myocardium. Nature Clinical Practice Cardiovascular Medicine **2**(11) (2005) 597–605
3. O'Donnell, T., Funka-Lea, G., Tek, H., Jolly, M.P., Rasch, M., Setser, R.: Comprehensive cardiovascular image analysis using MR and CT at Siemens Corporate Research. International Journal Of Computer Vision **70**(2) (2006) 165–178
4. Sampath, S., Prince, J.L.: Automatic 3D tracking of cardiac material markers using slice-following and harmonic-phase MRI. Magnetic Resonance Imaging **25**(2) (2007) 197–208
5. Axel, L.: Biomechanical dynamics of the heart with MRI. Annual Review Of Biomedical Engineering **4** (2002) 321–347
6. Bluemke, D. A. and Krupinski, E. A. and Ovitt, T. and Gear, K. and Unger, E. and Axel, L. and Boxt, L. M. and Casolo, G. and Ferrari, V. A. and Funaki, B. and Globits, S. and Higgins, C. B. and Julsrud, P. and Lipton, M. and Mawson, J. and Nygren, A. and Pennell, D. J. and Stillman, A. and White, R. D. and Wichter, T. and Marcus, F.: MR imaging of arrhythmogenic right ventricular cardiomyopathy: Morphologic findings and interobserver reliability. Cardiology **99**(3) (2003) 153–162
7. Hu, Z., Metaxas, D., Axel, L.: In vivo strain and stress estimation of the heart left and right ventricles from MRI images. Medical Image Analysis **7**(4) (2003) 435–444
8. Papademetris, X., Sinusas, A., Dione, D., Duncan, J.: Estimation of 3D left ventricular deformation from echocardiography. Medical Image Analysis **5**(1) (2001) 17–28
9. Papademetris, X., Sinusas, A.J., Dione, D.P., Constable, R.T., Duncan, J.S.: Estimation of 3-D left ventricular deformation from medical images using biomechanical models. IEEE Transactions on Medical Imaging **21**(7) (2002) 786
10. Sermesant, M., Coudiére, Y., Delingette, H., Ayache, N., J.Sainte-Marie, D. Chapelle, F.C., Sorine., M.: Progress towards model-based estimation of the cardiac electromechanical activity from ECG signals and 4D images. In: Modeling and Simulation for Computer-aided Medicine and Surgery. (2002)
11. Sermesant, M., Delingette, H., Ayache, N.: An electromechanical model of the heart for image analysis and simulation. IEEE Transactions in Medical Imaging **25**(5) (2006) 612–625
12. Sermesant, M., Moireau, P., Camara, O., Sainte-Marie, J., Andriantsimiavona, R., Cimrman, R., Hill, D., Chapelle, D., Razavi, R.: Cardiac function estimation from MRI using a heart model and data assimilation: Advances and difficulties. Medical Image Analysis **10**(4) (2006) 642–656
13. Moireau, P., Chapelle, D., Le Tallec, P.: Joint state and parameter estimation for distributed mechanical systems. Computer Methods in Applied Mechanics and Engineering **197** (2008) 659–677
14. Sundar, H., Sampath, R., Davatzikos, C., Biros, G.: Low-constant parallel algorithms for finite element simulations using linear octrees. In: Proceedings of SC2007. The SCxy Conference series in high performance networking and computing, Reno, Nevada, ACM/IEEE (2007)
15. Akcelik, V., Biros, G., Ghattas, O.: Parallel multiscale Gauss-Newton-Krylov methods for inverse wave propagation. In: Proceedings of the IEEE/ACM SC2002

Conference. The SCxy Conference series, Baltimore, Maryland, ACM/IEEE (November 2002)
16. Sundar, H., Shen, D., Biros, G., Litt, H., Davatzikos, C.: Estimating myocardial fiber orientation by template warping. In: International Symposium on Biomedical Imaging, Arlington, Virginia, IEEE (2006)
17. Shen, D.G., Sundar, H., Xue, Z., Fan, Y., Litt, H.: Consistent estimation of cardiac motions by 4D image registration. In: Medical Image Computing And Computer-Assisted Intervention - Miccai 2005, Pt 2. Volume 3750 of Lecture Notes In Computer Science. Springer-Verlag Berlin, Berlin (2005) 902–910
18. Gurtin, M.E.: An Introduction to Continuum Mechanics. Academic Press (1981)
19. Balay, S., Buschelman, K., Gropp, W.D., Kaushik, D., Knepley, M., McInnes, L.C., Smith, B.F., Zhang, H.: PETSc home page. http://www.mcs.anl.gov/petsc (2001)